

DLFormer: Enhancing Explainability in Multivariate Time Series Forecasting using Distributed Lag Embedding

Younghwi Kim^{1*}, Dohee Kim^{1*}, Sunghyun Sim^{2**}

¹*Safe & Clean Supply Chain Research Center, Pusan National University,
30-Jan-jeon Dong, Geum-Jeong Gu, 46241, Busan, South Korea*

²*Departments of Industrial Management & Big Data Engineering, Dong-eui University,
176 Eomgwang No, Gaya Dong 24, Busanjin Gu, 47340 Busan, South Korea ssh@deu.ac.kr*

** kim and kim are co-first authors, and sim is corresponding author*

Abstract. Most real-world variables are multivariate time series influenced by past values and explanatory factors. Consequently, predicting these time series data using artificial intelligence is ongoing. In particular, in fields such as healthcare and finance, where reliability is crucial, having understandable explanations for predictions is essential. However, achieving a balance between high prediction accuracy and intuitive explainability has proven challenging. Although attention-based models have limitations in representing the individual influences of each variable, these models can influence the temporal dependencies in time series prediction and the magnitude of the influence of individual variables. To address this issue, this study introduced DLFormer, an attention-based architecture integrated with distributed lag embedding, to temporally embed individual variables and capture their temporal influence. Through validation against various real-world datasets, DLFormer showcased superior performance improvements compared to existing attention-based high-performance models. Furthermore, comparing the relationships between variables enhanced the reliability of explainability.

Keywords: DLFormer, Distributed Lag Embedding, Multivariate Time series Forecasting, Explainable Multivariate Time series Forecasting Model, explainable Artificial Intelligence

1. Introduction

Time series data refers to the recorded continuum of sequence events delineated into the past, present, and future (Karim, Majumdar, & Darabi, 2020; Sim, Kim & Jeong, 2023) and encompass diverse domains such as healthcare (Petropoulos, Makridakis, & Stylianou, 2022), human social activities (Zhou, De la Torre, & Hodgins, 2012; Gong, Medioni, & Zhao, 2013), financial markets (Clements, Franses, & Swanson, 2004), and urban traffic management (Jin, Guo, Xu, Wang, & Wang, 2020, Sim, Park & Bae, 2022), wherein such data are continuously generated and stored (Kim, Sim, Yoon & Bae, 2023). Most of these data are multivariate, with multiple values at each time step (Wilms, Rombouts, & Croux, 2021; Lee, Kim & Sim, 2024). Consequently, utilizing multivariate time series data for knowledge extraction and application to societal issues is becoming increasingly prevalent, making multivariate time series prediction a challenging task widely regarded across most industries (Bidarkota, 1998).

The traditional approach to addressing multivariate time series prediction problems involves using statistical methods, such as vector autoregression and autoregressive distributed lag (ARDL) models (Qu, Huang, She, Liad, & Lai, 2024). However, statistical methods may struggle to capture complex sequence patterns in the data because of irregularities and nonlinearities among the features (Salinas, Flunkert, Gasthaus, & Januschowski, 2020). Therefore, layer-based deep-learning models incorporating recurrent layers (Rumelhart, Hinton, & Williams, 1986), long short-term memory layers (Hochreiter & Schmidhuber, 1997), gated recurrent units (Chung, Gulcehre, Cho & Bengio, 2014), and attention mechanisms (Vaswani, Shazeer, Parmar, Uszkoreit, Jones, Gomez, & Polosukhin, 2017) have been

widely explored in multivariate time series prediction (Catania, Grassi, & Ravazzolo, 2019). Deep learning-based models effectively learn sequential patterns in time series data and can outperform traditional statistical models, demonstrating superior prediction performance (Ortega, Otero, Solomon, Otero, & Fabregas, 2023). Another approach for improving the accuracy of multivariate time series prediction is to utilize models based on transformers, such as informers (Zhou, Zhang, Peng, Zhang, Li, Xiong, & Zhang, 2021) and autoformers (Wu, Xu, Wang, & Long, 2021). Transformer-based models effectively capture long- and short-term patterns in multivariate time series data and have surpassed traditional approaches in terms of prediction performance (Costa & Machado, 2023).

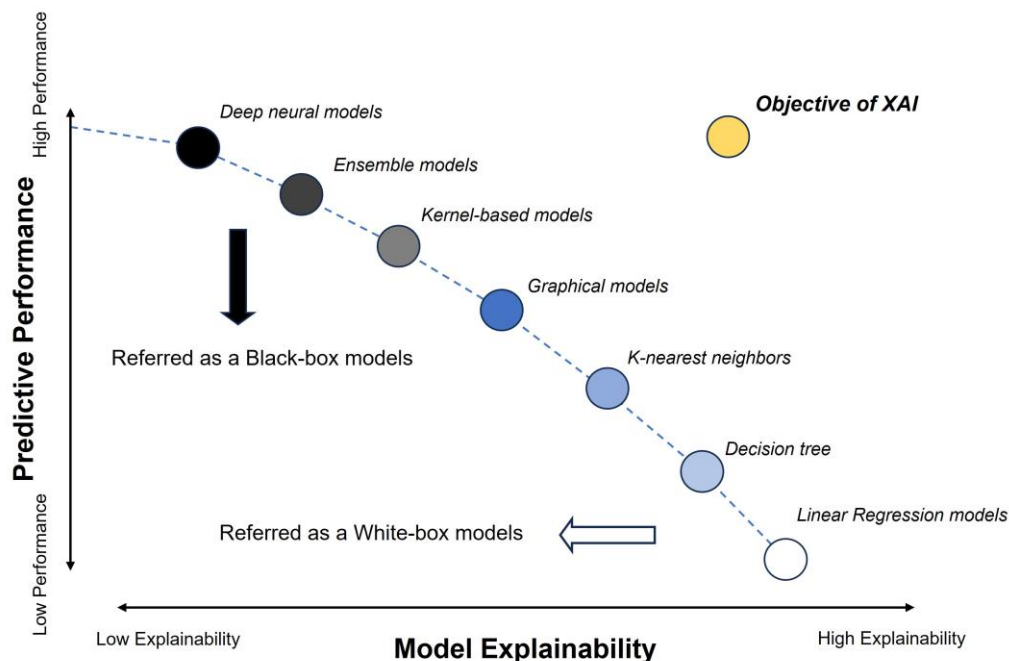


Fig. 1. Visualization of the tradeoff relationship between prediction accuracy and explainability in conventional ML

Recently, explainable artificial intelligence methods have become increasingly important in the business domain (Bellotti, Brigo, Gambetti, & Vrins, 2021), especially when applying predictive outcomes to interpret prediction results (Crook, Schlüter, & Speith, 2023). Fig. 1 illustrates the tradeoff between the complexity and interpretability of machine learning models. As the model complexity increases, the predictive performance tends to improve, but interpretability decreases (Rajapaksha, Bergmeir, & Hyndman, 2023). Transformer-based multivariate time series prediction models have higher accuracy but lower interpretability than traditional statistical models. Some studies have suggested that attention mechanisms can provide indirect evidence to explain the learning outcomes of a model to some extent (Makridakis, Hyndman, & Petropoulos, 2020; Vaswani et al., 2017; Bahdanau, Cho, & Bengio, 2014; Lee, Shin, & Kim, 2017). However, interpretation can be more challenging with multivariate time series prediction models that learn complex relationships between features and sequences (Lim, Arik, Loeff, & Pfister, 2021). Furthermore, in the attention operation process, such as in temporal fusion transformers (TFTs), the information of each feature is integrated into the embedding process, making it difficult to explain the influence of individual features. Hence, there are limitations in interpreting multivariate time series prediction models, such as TFT, as they can only extract the influence of the sequence on the prediction results.

We propose a DLFormer model, which allows for the simultaneous derivation of the prediction

results of the learned multivariate time series prediction model and the influence of features and sequences, overcoming the limitations of existing research. The aim is to achieve decent prediction performance compared to existing transformer-based time series prediction models while increasing the model’s interpretability. To achieve this goal, DLFormer employs the distributed lag embedding (DLE) method, which utilizes the distributed lag mechanisms commonly used in econometrics to simultaneously enhance the interpretability of features and sequences.

The main contributions of this study are as follows. 1) DLE in attention-based models facilitated the creation of structures that effectively captured the sequence effects of individual features in multivariate time series forecasting. 2) Our proposed method utilized interpretable multihead attention and DLE to create a structured representation that improved the learning style and provided explanations. 3) We compared DLFormer with state-of-the-art attention-based models using four large-scale multivariate time series datasets, demonstrating similar performance to prediction-focused attention-based models and improved performance over existing interpretable models. 4) In the experiments comparing DLFormer with existing explainable multivariate time series prediction models, DLFormer demonstrated its ability to effectively showcase the influence of features and sequences on the prediction outcomes. The analysis results also demonstrated its capability to enhance explainability.

The remainder of this paper is organized as follows. Section 2 provides a detailed analysis of the fundamental principles and limitations of current time series forecasting methods and elucidates the mechanisms behind explainable time series forecasting. Section 3 provides a detailed explanation of the proposed architecture and associated fundamental concepts. Section 4 describes the experimental setup, which includes four datasets, evaluation measures, and parameter settings for comparison with baseline models. as well as the experimental results. Section 5 validates the explanation by presenting examples of visualization and interpretation related to DLFormer forecasts. The accuracy of the explanations was verified by establishing linkages and making comparisons across different datasets. Finally, Section 6 consolidates the study's findings and explores potential directions for further research.

2. Related work

2.1. Multivariate Time series Forecasting Method

As machine learning has become more widely used in many industries, there is a growing tendency to use deep-learning models, either partially or wholly, to predict multivariate time series data (Li, Shang, & Wang, 2019; Sprangers, Schelter, & de Rijke, 2023; Elalem, Maier, & Seifert, 2023). Traditional approaches to forecasting multivariate time series data depend on vector autoregression (Sim, Kim, & Bae, 2023). In contrast, deep learning models that utilize recurrences provide a broader range of choices. The range of models includes simpler architectures such as recurrent neural networks (RNN) (Rumelhart, Hinton, & Williams, 1986), long short-term memory (LSTM) (Hochreiter & Schmidhuber, 1997), and gated recurrent units (GRU) (Chung, Gulcehre, Cho, & Bengio, 2014), as well as more complex methods such as long- and short-term time series networks that utilize a combination of convolutional neural network and recursive skip connections to accurately record sequence patterns, including long- and short-term patterns, at various times (Lai, Chang, Yang, & Liu, 2018). However, almost all these models lack specific statements regarding inherent explainability (Pantiskas, Verstoep, & Bal, 2020; Katsikopoulos, Şimşek, Buckmann, & Gigerenzer, 2022).

The transformer-based model, incorporating a multi-head self-attention mechanism, has recently demonstrated outstanding results in natural language processing and computer vision (Zeng, Chen, Zhang, & Xu, 2023). Consequently, there is a growing demand for research on time series modeling

using transformer-based methods (Zhou et al., 2021; Wu, Xu, Wang, & Long, 2021;). Informer (Zhou et al., 2021) surpasses the performance of existing methods by employing KL-divergence-based *ProbSparse* Attention while effectively handling large input sequences through self-attention distillation. Autoformer (Wu, Xu, Wang, & Long, 2021) achieves outstanding results at the subseries level by integrating the series decomposition block as internal operators and implementing an efficient autocorrelation mechanism. These models exhibit outstanding results in time series prediction, confirming the efficacy of attention in time series prediction (Wang, Hyndman, Li, & Kang, 2023). However, the current method of mixing factors in the input makes it difficult to determine the significance of individual features at specific time steps despite the insights that can be obtained from analyzing attention outcomes (Lim, Arik, Loeff, & Pfister, 2021)

2.2. Explainable Method for Multivariate Time series

ARDL is a traditional statistical approach for ensuring explanatory power in multivariate time series models. The method uses the lag variables of the target and explanatory features in the regression structure and has been extensively used to assess long- and short-term relationships by estimating regression coefficients during forecasting (Bildirici & Türkmen, 2015; Raza, Shahzad, Tiwari, & Shahbaz, 2016). However, certain studies indicate that conventional econometric models such as ARDL frequently depend on linear assumptions, which reduce forecasting accuracy by neglecting to incorporate concealed nonlinear patterns in time series data (Bentzen & Engsted, 2001).

Recent research has actively explored learned attention scores within attention-based models to analyze the relationship between the encoder input and decoder output, finding applications in multivariate time series prediction studies (Lim, Arik, Loeff, & Pfister, 2021; Pantiskas, Verstoep, & Bal, 2020). TFTs (Lim, Arik, Loeff, & Pfister, 2021) have exhibited remarkable efficacy in long short-term forecasting by inherently offering interpretability and harnessing observed and known inputs. Furthermore, by employing an interpretable multi-head attention mechanism that shares attention across each head in an ensemble manner, diverse sequence patterns learned across multiple heads were integrated to derive the overall sequence influence. Although significant time points in time series data are crucial, accurately representing the influence of various features is equally important. To address this, selecting components directly affecting the prediction for static and time-dependent covariates involves passing through flattened inputs and external context at each time step, followed by a gated residual network (GRN) and softmax functions, generating variable selection weights. These weights modify the transformed input passing through the GRN by applying matrix multiplication and weighted summation to accurately depict the influence of the features at each time step. TFT has demonstrated interpretability in time series predictions and the explainability of interpretable multihead attention and variable selection networks in different domains (Wu, Wang, & Zeng, 2022; López Santos, García-Santiago, Echevarría Camarero, Blázquez Gil, & Carrasco Ortega, 2022). However, interpretable multihead attention in TFT combines all features during computation and cannot capture the sequence influence of individual features.

A temporal attention convolutional neural network (TACN) (Pantiskas, Verstoep, & Bal, 2020) combines attention with temporal convolutional networks (TCN) to create an interpretable model. The input was abstracted into filter dimensions for each feature using multiple TCN blocks. Subsequently, the output data were learned by transforming them into output dimensions. Subsequently, it determines the influence of the sequence on the relationship between the input and output by comparing the original input with the learned output data. However, regarding this explanation as a comprehensive

representation of the sequence significance of individual features is impractical.

3. DLFormer

Fig. 2 shows the overall architecture of DLFormer. DLFormer consists of n encoder and m decoder blocks, each containing h interpretable multihead attention (IMH). Additionally, a new embedding method called DLE was applied to learn the relationships between individual features and sequences. DLFormer provides the influence of feature and sequence simultaneously after multivariate time series prediction, unlike existing explainable multivariate time series prediction models.

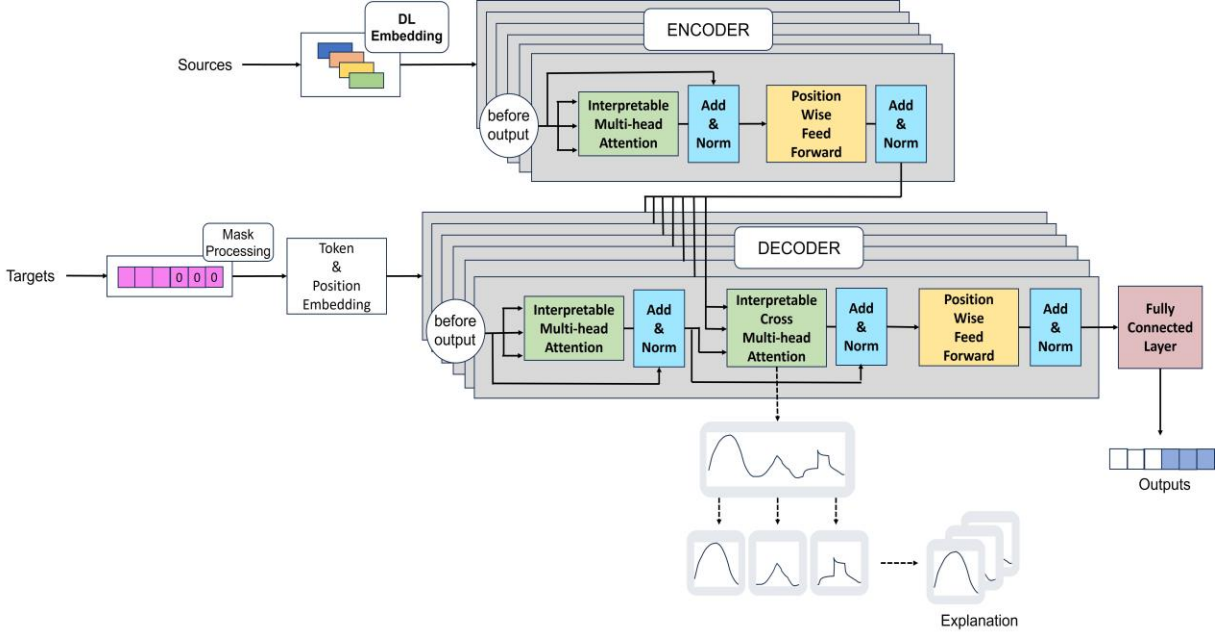


Fig. 2 Overall structure of DLFormer

In Section 3.1, we introduce DLE, laying the groundwork for understanding DLFormer. Section 3.2 presents the encoder and decoder in DLFormer, while Section 3.3 delves into the training mechanism. Finally, in Section 3.4, we explore an interpretable method using the DLFormer. The mathematical notations used in our modeling and methods are summarized in Table 1.

Table 1. Overview of the notations used in DLFormer

Notation	Description	Notation	Description
k	Number of features	l	Index of encoder & decoder block
L	Size of distributed lag	r	Reference length of target y
p_G	$k \times L$, Size of total sequence	T	Forecasting horizon
p	Sequence position	IMH	Interpretable multi-head attention
d_E	Size of embedding dimensions	$ICMH$	Interpretable cross multi-head attention
d_A	Size of attention dimensions	$PWFF$	Position wise feed forward
d	Index of embedding dimensions	Z_l^1	Output in the IMH of l^{th} encoder block
v	Numerical for periodicity	Z_l^2	Output in the $PWFF$ of l^{th} encoder block
h	Number of attention heads	S_l^1	Output in the IMH of l^{th} decoder block
n	Number of encoder block	S_l^2	Output in the $ICMH$ of l^{th} decoder block
m	Number of decoder block	S_l^3	Output in the $PWFF$ of l^{th} decoder block

3.1. Distributed Lag Embedding for DLFormer

To forecast the k multivariate time series X , the input for the k^{th} feature utilizing a past sequence of length L is given by Eq. (1)

$$X^k = \{x_1^k, \dots, x_L^k\} \quad (1)$$

X , which contains the values for all the features, encompasses X^1 to X^k . The conventional attention mechanism effectively captures the sequence relationships in X by embedding them according to time. However, this structure embeds individual features x_L^1 to x_L^k without capturing the sequence relationships of individual features. To overcome this problem, we applied DLE to the attention mechanism as an input, individually embedding all lagged values of each feature in the time series data X . Before passing through the learned embedding layer, $X_{DL} \in \mathbb{R}^{p_G \cdot 1}$, which consists of lagged values of k features as individual features, can be represented using Eq. (2). For brevity, we denote $k * L$ as p_G .

$$X_{DL} = \{x_1^1, \dots, x_L^1, \dots, x_1^k, \dots, x_L^k\} \quad (2)$$

We projected X_{DL} onto a learnable distributed lag vector representing individual feature sequences using a linear layer with dimensionality d_E . In addition, to inject positional information for individual feature sequences and utilize sequence order information, we use sequence position embeddings (SPE) to propose global and local SPE (GSPE and LSPE, respectively), defined as follows:

$$SPE_{(p,2d)} = \sin(p/v^{2d/d_G}) \quad (3)$$

$$SPE_{(p,2d+1)} = \cos(p/v^{2d/d_G}) \quad (4)$$

where $p \in \{1, \dots, p_G\}$ represents the sequence position, $d \in \{0, \dots, d_E/2\}$ represents the index of the embedding dimension, and constant v determines the period of the periodic function. Applying sine and cosine functions of different frequencies to alternate the even and odd dimensions of each embedding dimension ensures that each sequence has a unique position embedding vector. We inject patterns for the overall feature sequence and use GSPE and local LSPE to inject time patterns for individual features. The $GSPE_{(p,d)}$ represents $SPE_{(p,d)}$ with $p \in \{1, \dots, p_G\}$ and $d \in \{1, \dots, d_G/2\}$. The $LSPE_{(p,d)}$ is a concatenation of k $SPE_{(p,d)}$ with $p \in \{1, \dots, p_L\}$ and $d \in \{1, \dots, d_L/2\}$, where $p_L = L$ is the distributed lag size. The equation for $LSPE$ is given by Eq. (5). The GSPE and LSPE representation sizes are d_G and d_L , respectively.

$$LSPE_{(p,d)}^k = \text{Concat}(SPE_{(p,d)}^1, \dots, SPE_{(p,d)}^k) \quad (5)$$

To incorporate the concepts of GSPE and LSPE, they were summed to create a DLE. Therefore, the DLE used as the encoder input for DLFormer is represented using Eq. (6). DLV represents the values after passing through the learnable embedding layer from the original X_{DL} .

$$DLE = DLV + GSPE_{(p,d)} + LSPE_{(p,d)}^k \quad (6)$$

Fig. 3 intuitively demonstrates the operational process of DLE. Individually embedding multiple feature sequences allows for capturing the influence of individual feature sequences in forecasting from

a higher representation perspective. The process of converting the original time series dataset into DLE vectors is outlined in Algorithm 1 and was applied to all samples in the experiments. DLE is a crucial element in DLFormer, ensuring explainability by individually identifying the sequence influence of each feature in attention.

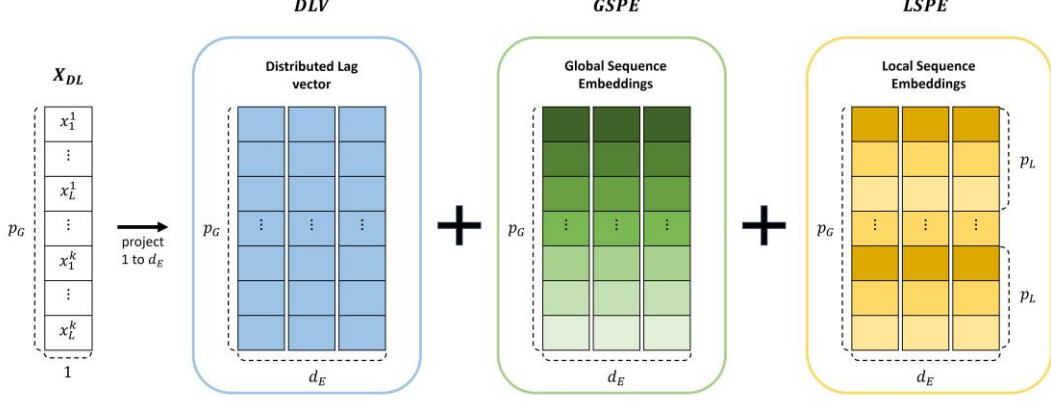


Fig. 3 Visualization of Distributed Lag Embedding

Algorithm 1. Distributed Lag Embedding

Input: Time series data X
Output: DLFormer input DLE

- 1: $X^{DL} \leftarrow []$
- 2: **for** $i \leftarrow 1$ to k **do**
- 3: $X^{DL}.append(X^i)$
- 4: $DLV \leftarrow \text{projection } X^{DL}$
- 5: $DLE \leftarrow DLV + GSPE + LSPE$ using Eq. (6)
- 6: **return** DLE

3.2. Structure of DLFormer

DLFormer consists of n encoder and m decoder blocks; each encoder and decoder contain h interpretable multi-head attention (IMH). Attention operations within the IMH employ a scaled dot-product attention mechanism as follows:

$$A(Q, K) = \text{Softmax}(QK^T / \sqrt{d_A}) \quad (7)$$

$$\text{Attention}(Q, K, V) = A(Q, K)V \quad (8)$$

$$H = \text{Attention}(QW^Q, KW^K, VW^V) \quad (9)$$

where $W^Q, W^K, W^V \in \mathbb{R}^{d_E \times d_A}$ are the weight matrices for Q, K , and V applied within each head, respectively, d_A represents the dimensionality of the representations of Q, K , and V used within a single-head attention operation. Eq. (7) represents the attention score. To prevent attention scores from becoming too large after matrix multiplication of inputs Q and K , we scaled them by $1/\sqrt{d_A}$ before applying the softmax function. Accordingly, as shown in Eq. (8), matrix multiplication with V follows. Ultimately, the result of the single-head attention, in Eq. (9), consists of operations where each weight W is multiplied with Q, K , and V . Utilizing this approach to reflect learning across various heads, IMH employs an averaging method as follows.

$$\bar{A}(Q, K) = \frac{1}{h} \sum_{i=1}^h A(QW_i^Q, KW_i^K) \quad (10)$$

$$\bar{H} = \bar{A}(Q, K)VW^V \quad (11)$$

$$\bar{H} = \frac{1}{h} \sum_{i=1}^h \text{Attention}(QW_i^Q, KW_i^K, VW^V) \quad (12)$$

$$\text{IMH}(Q, K, V) = \bar{H}W^H \quad (13)$$

IMH has h sets of weights, W^Q , W^K for Q and K , respectively, as shown in Eq. (10). Additionally, W^V , shared across all h heads, represents the weights applied to V . Therefore, the average attention is computed as shown in Eq. (11). This allowed each head to learn different temporal patterns (Eq. (12)). Finally, \bar{H} is multiplied by W^H , which represents the weights used for the final linear mapping to produce the IMH output. This can effectively integrate the learning patterns of multiple heads compared to the traditional multihead attention approach for a clearer representation of the sequence influence of K on Q during training.

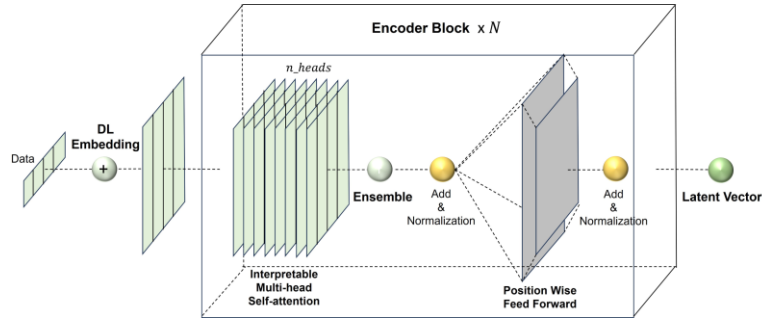


Fig. 4 Encoder block structure

Fig. 4 shows the encoder block structure comprising the introduced IMH and position wise feed forward (PWFF) units. DLE uses Q, K , and V inputs to generate a latent vector representing the importance of individual feature sequences. This vector is later used in the cross attention of the decoder to derive the relevance importance between the output sequence of the target and latent vectors. The l^{th} encoder block is expressed using Eqs. (14) and (15) as follows:

$$Z_l^1 = \text{IMH}(Z_{l-1}^2, Z_{l-1}^2, Z_{l-1}^2) + Z_{l-1}^2 \quad (14)$$

$$Z_l^2 = \text{PWFF}(Z_l^1) + Z_l^1 \quad (15)$$

$Z_l^2 (1 \leq l \leq n)$ represents the output of the l^{th} encoder block, where Z_0^2 corresponds to the input of DLFormer, which is DLE. Z_n^2 represents the latent vector in Fig. 4, which is used as K and V in the decoder to understand the influence of the individual features within the DLE on the target sequence.

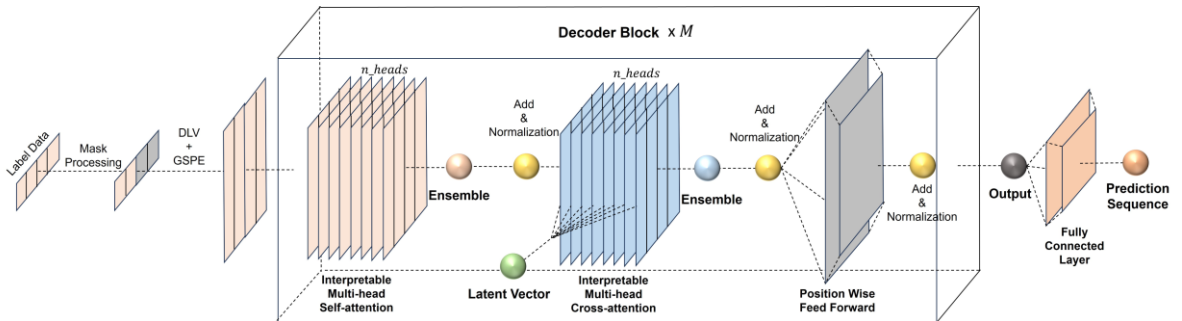


Fig. 5 Decoder block structure

Fig. 5 shows the decoder block structure comprising an IMH, an interpretable cross multi-head attention (ICMH), and a PWFF. Before embedding, the decoder input was structured as follows:

$$y_{de} = \text{Concat}(y_r, y_r^0) \quad (16)$$

where y_r represents the previous target sequence values from the forecasting time point up to the reference length r . y_r^0 is the masked value of the future sequences for the forecasting horizon T and is set to 0 from the forecasting time point. To incorporate the influence of previous sequences during the attention process for forecasting horizon T , we concatenated them. The concatenated values, denoted as y_{de} , are passed through the embedding layer and projected onto d_E dimensions. Subsequently, to inject target sequence information, $SPE_{(p,d)}$ with $p \in \{1, \dots, T + r\}$ and $d \in \{1, \dots, \}$ is added to form the decoder input $S_{0,3}$. The l^{th} decoder block is represented using Eqs. (17) to (19).

$$S_l^1 = \text{IMH}(S_{l-1}^3, S_{l-1}^3, S_{l-1}^3) + S_{l-1}^3 \quad (17)$$

$$S_l^2 = \text{ICMH}(S_l^1, Z_n^2, Z_n^2) + S_l^1 \quad (18)$$

$$S_l^3 = \text{PWFF}(S_l^2) + S_l^2 \quad (19)$$

$S_l^3 (1 \leq l \leq m)$ represents the output of the l^{th} Decoder, the input is the output of the previous decoder block, and the initial decoder input is S_0^3 . ICMH is additionally applied in the decoder, as described in Eq. (18), where S_l^1 serves as Q , and the latent vector Z_n^2 derived from the encoder serves as K and V . Thus, the dependency between the individual feature sequences of the latent vector and the target sequence is captured. Subsequently, the decoder output passes through FFN, similar to the encoder, generating output S_l^3 . Finally, the decoder output S_M^3 is transformed into the prediction result through a fully connected layer comprising two linear layers and an intermediate activation function to project it from d_E to 1.

Thus, the proposed DLFormer utilizes DLE to capture the complex relationship between the input and output sequences and represent all the individual features within the attention structure. In addition, it adopts an IMH-based model architecture to incorporate representations from multiple heads.

3.3. Learning Mechanism

Algorithm 2 represents the learning mechanism of DLFormer. The output is the DLFormer model F_φ with optimized parameters φ . The input comprises N samples of multivariate time series X with k individual features and the reference sequence y_r for the target feature to be predicted. These were sequentially transformed into Z_0^2 and S_0^3 of size d_E for model input using **Algorithm 1 and Equation (16)**. The transformed inputs then pass through n encoder and m decoder blocks.

We employed the mean squared error (MSE) as the loss function, as shown in **Eq. (20)**. The weights were trained using the Adam Optimizer with backpropagation of errors to minimize MSE by adjusting φ . Training was conducted over a specified number of batches. Furthermore, iterating over a designated number of epochs, we selected the optimal DLFormer model (F_φ) based on the highest accuracy achieved on the validation set.

$$MSE = \frac{1}{N} \sum_{i=1}^N (y_i - \hat{y}_i)^2 \quad (20)$$

Algorithm 2. Training procedure of DLFormer

Input: Time series data X, y^r
Output: F_φ

- 1: **for** 1 to *Epoch* **do**
- 2: $Z_0^2 \leftarrow$ DLE using Algorithm 1
- 3: $S_0^3 \leftarrow$ embedded $y_{de} + SPE_{(p,d)}$ with $p \in \{1, \dots, T + r\}$ and $d \in \{1, \dots, d_E/2\}$
- 4: **for** $l = 1$ to n **do** \triangleright Encoder
- 5: $Z_l^1 \leftarrow IMH(Z_{l-1}^2, Z_{l-1}^2, Z_{l-1}^2) + Z_{l-1}^2$ using Eq. (14)
- 6: $Z_l^2 \leftarrow FFN(Z_l^1) + Z_l^1$ using Eq. (15)
- 7: **for** $l = 1$ to m **do** \triangleright Decoder
- 8: $S_l^1 \leftarrow IMH(S_{l-1}^3, S_{l-1}^3, S_{l-1}^3) + S_{l-1}^3$ using Eq. (16)
- 9: $S_l^2 \leftarrow IMH(S_l^1, Z_n^2, Z_n^2) + S_l^1$ using Eq. (17)
- 10: $S_l^3 \leftarrow FFN(S_l^2) + S_l^2$ using Eq. (18)
- 11: $\hat{Y} \leftarrow FCL(S_m^3)$ \triangleright projection S_m^3 to \hat{Y}
- 12: $Loss_\varphi \leftarrow MSE(Y, \hat{Y})$ using Eq. (20)
- 13: $\varphi \leftarrow \varphi - \eta \nabla_\varphi Loss_\varphi$

3.4. Explanation

The explanation for predictions in the proposed DLFormer elucidates the influence of individual features and sequences on future time steps. Therefore, it leverages the attention weights from the ICMH within the DLFormer decoder block, as follows:

$$A_{explanation} = \frac{1}{N} \bar{A}(S_{m,1}, Z_{n,2}) \quad (21)$$

where N is the number of data points. Similarly, we derived the influence of individual features and sequences on the prediction through the operation in Eq. (21) between the latent vector $Z_{n,2}$ obtained through the encoder and $S_{m,1}$ from the last decoder block. We also extract the attention weights corresponding to the last row of the output sequence. Furthermore, averaging is performed to assess the average influence across all samples. Algorithm 3 provides a comprehensive overview of extracting the attention weights for predictions.

Algorithm 3. Extract Explanation of DLFormer

Input: Time series data X, y^r
Output: $A_{explanation}$

- 1: $Z_0^2 \leftarrow$ DLE using Algorithm 1
- 2: $S_0^3 \leftarrow$ embedded $y_{de} + SPE_{(p,d)}$ with $p \in \{1, \dots, L\}$ and $d \in \{1, \dots, d_E/2\}$
- 3: **for** $l = 1$ to n **do** \triangleright Encoder
- 4: $Z_l^1 \leftarrow IMH(Z_{l-1}^2, Z_{l-1}^2, Z_{l-1}^2) + Z_{l-1}^2$ using Eq. (14)
- 5: $Z_l^2 \leftarrow FFN(Z_l^1) + Z_l^1$ using Eq. (15)
- 6: **for** $l = 1$ to m **do** \triangleright Decoder
- 7: $S_l^1 \leftarrow IMH(S_{l-1}^3, S_{l-1}^3, S_{l-1}^3) + S_{l-1}^3$ using Eq. (16)
- 8: $S_l^2 \leftarrow IMH(S_l^1, Z_n^2, Z_n^2) + S_l^1$ using Eq. (17)
- 9: $S_l^3 \leftarrow FFN(S_l^2) + S_l^2$ using Eq. (18)
- 10: $A_{explanation} \leftarrow$ Sample average to $\bar{A}(S_m^1, Z_n^1)$ using Eq. (21)

4. Experiments

We performed comprehensive experiments to compare and evaluate the predictive performance of DLFormer. These studies involved four multivariate time series datasets, including collected datasets for explainability and publicly available benchmark datasets.

4.1. Data Description

The four multivariate time series datasets used in our experiment consisted of one real-world dataset (Air Quality) and three public benchmark datasets (ETTh1, ETTh2, and Weather). To ensure consistency, we divided the datasets into training, valid, and test datasets in ratios of 60%, 20%, and 20%, respectively, for each experiment. In addition, the forecasting horizon T was defined as $T \in \{1, 3, 6, 12\}$. **Table 2** provides a concise overview of the four datasets, which consist of multiple variables observed over time.

Table 2. Statistic of the four benchmark datasets for the explainable time series forecasting

Datasets	ETTh1	ETTh2	Air Quality	Weather
Number of features	7	7	7	7
Number of rows	17420	17420	9357	52696
Time interval	1 h	1 h	1 h	10 min

4.2. Experiments Setting

4.2.1. Baseline

We selected five baseline models for comparison in our multivariate time series forecasting experiments. The models used were LSTM, an RNN-based model, two attention-based models, namely Informer and Autoformer, and two interpretable models, TFT and TACN.

4.2.2. Implementation Details

The five baseline models used in the comparative experiment and DLFormer were implemented using PyTorch. For each model, the parameters were varied to determine the best-performing configuration: 1) LSTM: We increased the number of layers from one to five and varied the hidden dimension size among 64, 128, 256, and 512. 2) Autoformer: We used 512 embedding dimensions and a moving average size of 25. We increased the number of autocorrelation heads from two to eight and varied the number of encoders and decoders from one to six. 3) Informer: We used embedding dimensions of 512. The number of attention heads varied from 2 to 8, and the numbers of encoders and decoders ranged from 1 to 6. 4) TFT: The hidden dimensions were 64, 128, 256, and 512. The number of attention heads increased from two to eight, and the number of LSTM layers ranged from one to five. 5) TACN: We used a kernel size of 3 and varied the channel sizes to 64, 128, 256, and 512. In addition, we increased the number of layers from one to five.

Due to the constraints of our experimental environment, we adjusted the input sequence L for our DLFormer in the range $L \in \{3, 6, 12, 24\}$. Through experimentation, d_E was determined to be 128, whereas d_A was set to 16. The number of attention heads h was set to eight. The target reference length was set equal to the forecasting horizon T . We set the number of encoders (N) and decoders (M) to 6 and v to 10,000 to determine the periodicity of SPE . Additionally, the activation function for the embedding layer and MLP used for the output in the decoder was set to ReLU (Nair & Hinton, 2010). The training was performed using the Adam optimizer (Kingma & Ba, 2014) with an initial learning

rate of 10^{-4} and MSE loss. The batch size was set to 64 and early stopping was employed to terminate the training if the loss function of the validation set did not improve after 50 consecutive updates within 200 epochs.

4.2.3. Metric & Platform

To evaluate the performance of each model based on distance and direction, we employed the traditional time series prediction metrics, such as the root mean square error (RMSE), r-squared score (R^2), and dynamic time warping (DTW) (Berndt & Clifford, 1994), to indicate the similarity of patterns between two time-series. All our model experiments were trained on a single NVIDIA TITAN RTX 24GB GPU.

4.3. Performance by Parameter

In DLFormer, we set the crucial hyperparameter input sequence length L to explain significant past time steps for the predictions. This can lead to improved prediction performance depending on the data characteristics and can also determine the size of the past values to be evaluated. In our experiments, we constrained $L \in \{3, 6, 12, 24\}$ and evaluated the model’s performance and efficiency.

Table 3. Forecasting Error based on Lag in DLFormer

Method		3 Lag			6 Lag			12 Lag			24 Lag		
Metric		RMSE	R2	DTW	RMSE	R2	DTW	RMSE	R2	DTW	RMSE	R2	DTW
Air Quality	1	0.76	0.68	16.01	0.71	0.71	14.66	0.68	0.72	15.40	0.64	0.76	17.24
	3	1.29	-0.78	28.41	1.25	-0.68	28.02	1.07	0.01	26.64	1.02	0.24	25.24
	6	1.40	-4.60	38.00	1.32	-2.93	35.75	1.19	-0.65	29.76	1.12	0.02	25.68
	12	1.30	-2.72	33.61	1.30	-2.26	33.10	1.17	-0.61	30.04	1.19	-0.25	27.06
ETTh1	1	0.68	0.95	13.228	0.68	0.95	13.42	0.67	0.95	12.44	0.68	0.95	14.30
	3	1.36	0.81	30.99	1.32	0.82	29.87	1.22	0.84	28.47	1.21	0.85	27.48
	6	2.06	0.52	49.01	1.82	0.63	39.02	1.63	0.70	37.44	1.68	0.67	38.83
	12	2.76	0.20	60.12	2.80	0.20	60.38	2.10	0.36	50.22	2.25	0.31	53.39
ETTh2	1	1.09	0.98	40.78	1.09	0.98	40.07	1.06	0.98	38.62	0.95	0.99	35.94
	3	3.15	0.90	70.00	3.37	0.88	75.53	2.96	0.91	71.69	2.55	0.93	61.80
	6	6.52	0.50	142.08	6.24	0.46	139.76	5.67	0.58	129.78	4.76	0.72	114.15
	12	8.24	0.15	174.55	7.03	0.35	159.04	5.29	0.70	122.43	5.30	0.69	127.10
Weather	1	0.19	0.99	9.05	0.21	0.99	9.91	0.19	0.99	9.06	0.22	0.99	9.92
	3	0.46	0.99	20.45	0.50	0.98	21.36	0.57	0.98	23.80	0.55	0.98	23.10
	6	0.86	0.96	41.87	0.95	0.96	44.59	1.00	0.95	48.01	1.02	0.95	47.79
	12	1.86	0.84	94.00	1.97	0.83	104.12	2.20	0.79	111.97	2.26	0.79	106.64

Table 3 summarizes the prediction performance of DLFormer based on hyperparameter L . The best prediction results for each dataset vary with L , indicating that the range of past values that contribute to the prediction varies depending on the characteristics and time interval of each dataset. For example, the Air Quality, ETTh1, ETTh2, and Weather datasets demonstrate the best prediction performance at

$L = 24, 12, 24,$ and $3,$ respectively. Air Quality, ETTH1, and ETTh2 datasets demonstrated the need to capture influential patterns from previous longer sequences collected at hourly intervals. Increasing the length of the input sequences, particularly to 12 h for Air Quality, 12 h for ETTH1, and 24 h for ETTh2, improved prediction accuracy. In contrast, the Weather dataset, which is more volatile and requires more complex predictions, showed better results when using 30-min old data collected at 10-min intervals, compared to longer time windows. Based on the best results, we compared them with five baseline models.

4.4. Experimental Results

Tables 4–7 summarize the multivariate time series forecasting experimental results of DLformer and five baseline models for each dataset in terms of the mean RMSE, R^2 , and DTW obtained from 30 repeated experiments under the same conditions. Additionally, to indicate the average ranking of prediction performance by method, rankings are assigned for each metric (RMSE, R^2 , DTW) across all ranges of $T \in \{1, 3, 6, 12\}$; the average rankings are presented at the bottom of each table. The superior average ranking results are highlighted in bold.

Table 4 presents the prediction performance results for the Air Quality dataset. Overall, the attention-based models demonstrated an outstanding prediction performance. Except for a few cases in R^2 and DTW metrics, DLFormer shows the best prediction performance for most T among the six models. Although DLFormer slightly lagged behind the TACN model in RMSE metric, it outperformed the other models in most cases.

Table 5 presents the predicted performance results for the ETTh1 dataset. The TACN model demonstrated outstanding performance, with the highest average rankings across all metrics. However, DLFormer exhibited excellent overall performance and outperformed other models, except TACN, in most cases.

Table 6 presents the results for the ETTh2 dataset. DLFormer achieved the second-highest average rankings in R^2 and DTW metrics. In particular, DLFormer exhibits excellent performance at $T=12$ but lags behind TFT and TACN models in terms of RMSE. TFT and TACN had similar overall rankings.

Table 7 presents the results for the Weather dataset. Similar to Table 5, the TACN model demonstrated the highest prediction performance in most cases, with the highest average ranking across all metrics, followed by DLFormer, Autoformer, TFT, Informer, and LSTM models.

Figs. 6–9 present the results in Tables 4–7 as bar graphs for each dataset across the three metrics. The plots show that DLFormer consistently maintained a high level of predictive performance in most cases and exhibited the best performance in some cases. Thus, it demonstrates comparable predictive performance to state-of-the-art attention-based models without performance degradation despite their combined structure incorporating the proposed explainability mechanism, DLE, and a simple attention mechanism

Table 4 Forecasting results for each model using the Air Quality Dataset

Model		LSTM			TFT			TACN			Informer			Autoformer			Ours		
Metric		RMSE	R ²	DTW	RMSE	R ²	DTW	RMSE	R ²	DTW	RMSE	R ²	DTW	RMSE	R ²	DTW	RMSE	R ²	DTW
ETTh1	1	1.21	-2.79	41.45	1.01	-0.14	28.09	0.67	0.68	16.46	0.68	0.62	19.20	0.78	0.67	19.24	0.64	0.76	17.24
	3	1.30	-5.10	46.61	1.13	-0.75	32.19	0.99	0.15	24.62	1.01	-0.05	28.44	1.05	0.26	25.48	1.02	0.24	25.24
	6	1.36	-3.01	44.10	1.35	-4.43	42.08	1.09	-0.50	29.32	1.20	-0.05	28.22	1.22	-0.13	27.55	1.12	0.02	25.68
	12	1.38	-6.18	47.36	1.44	-13.39	49.11	1.23	-1.35	33.18	1.18	-0.67	28.82	1.42	-0.57	28.60	1.19	-0.25	27.06
AVG Rank		5.5	5.5	5.75	5.25	5.5	5.25	1.75	3.25	2.5	2.25	3.25	3.25	4.25	2.25	2.75	2	1.25	1.5

Table 5 Forecasting results for each model using the ETTh1 Dataset

Model		LSTM			TFT			TACN			Informer			Autoformer			Ours		
Metric		RMSE	R ²	DTW	RMSE	R ²	DTW	RMSE	R ²	DTW	RMSE	R ²	DTW	RMSE	R ²	DTW	RMSE	R ²	DTW
ETTh1	1	2.33	0.33	70.16	0.92	0.92	21.88	0.67	0.96	9.58	1.13	0.88	35.95	0.92	0.92	28.51	0.67	0.95	12.44
	3	3.32	-1.89	95.97	1.13	0.88	27.30	1.12	0.88	15.31	1.95	0.71	66.80	1.45	0.80	41.11	1.22	0.84	28.47
	6	3.35	-1.80	74.77	1.60	0.74	38.17	1.53	0.76	28.45	2.65	0.49	79.48	2.02	0.60	52.30	1.63	0.70	37.44
	12	3.75	-7.04	99.32	2.30	0.35	54.20	1.99	0.58	40.93	3.29	-0.40	72.45	2.83	0.17	68.86	2.10	0.36	50.22
AVG Rank		6	6	5.75	2.75	2.625	2.75	1	1.25	1	5	5	5	3.75	3.75	4	2.5	2.5	2.25

Table 6 Forecasting results for each model using the ETTh2 Dataset

Model		LSTM			TFT			TACN			Informer			Autoformer			Ours		
Metric		RMSE	R ²	DTW	RMSE	R ²	DTW	RMSE	R ²	DTW	RMSE	R ²	DTW	RMSE	R ²	DTW	RMSE	R ²	DTW
ETTh1	1	5.70	0.53	170.85	1.50	0.97	46.19	0.95	0.99	32.40	1.93	0.95	60.27	1.20	0.98	45.25	0.95	0.99	35.94
	3	7.42	0.07	228.91	2.00	0.96	59.23	2.30	0.95	49.35	4.26	0.79	117.89	2.37	0.94	70.69	2.55	0.93	61.80
	6	7.61	-0.37	232.28	3.36	0.88	92.85	3.77	0.86	90.20	7.72	0.12	173.88	3.86	0.85	103.49	4.76	0.72	114.15
	12	8.57	-1.11	291.51	5.08	0.69	133.93	5.73	0.64	146.02	8.75	-0.70	178.01	5.45	0.66	127.95	5.30	0.69	127.10
AVG Rank		5.5	6	6	1.75	2	2.75	2.5	2.5	1.75	5.5	5	5	3	3	3	2.75	2.5	2.5

Table 7 Forecasting results for each model using the Weather Dataset

Model		LSTM			TFT			TACN			Informer			Autoformer			Ours		
Metric		RMSE	R ²	DTW	RMSE	R ²	DTW	RMSE	R ²	DTW	RMSE	R ²	DTW	RMSE	R ²	DTW	RMSE	R ²	DTW
ETTh1	1	2.55	0.66	134.53	0.41	0.99	14.60	0.17	0.99	6.40	0.35	0.99	15.43	0.27	0.99	14.71	0.19	0.99	9.05
	3	3.13	0.29	151.88	0.57	0.98	19.35	0.40	0.99	10.68	0.69	0.97	29.04	0.58	0.98	28.99	0.46	0.99	20.45
	6	2.12	0.72	107.06	1.03	0.95	34.91	0.68	0.98	17.40	1.18	0.93	50.31	0.81	0.97	34.57	0.86	0.96	41.87
	12	2.86	0.40	179.90	1.77	0.83	72.10	1.18	0.94	32.45	2.50	0.62	107.55	1.70	0.88	85.94	1.86	0.84	94.00
AVG Rank		6	6	6	3.75	4.25	2.5	1	1.125	1	4.75	4.75	5	2.75	2.5	3.25	2.75	2.375	3.25

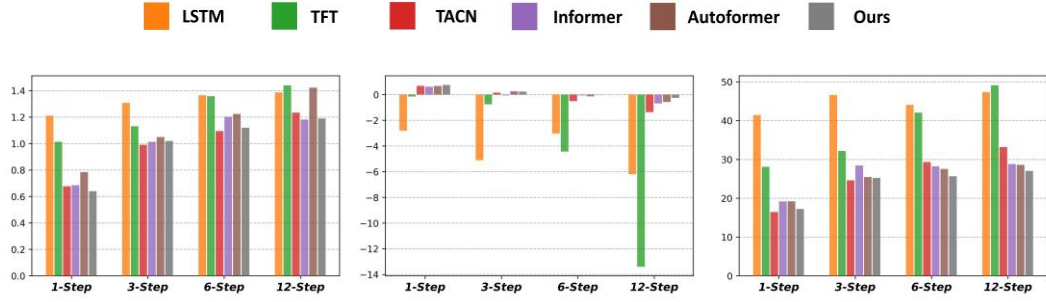


Fig. 6 Average performance results of 30 models for the Air Quality dataset. RMSE: root mean square error, R^2 : R-squared, and DTW: dynamic time warping

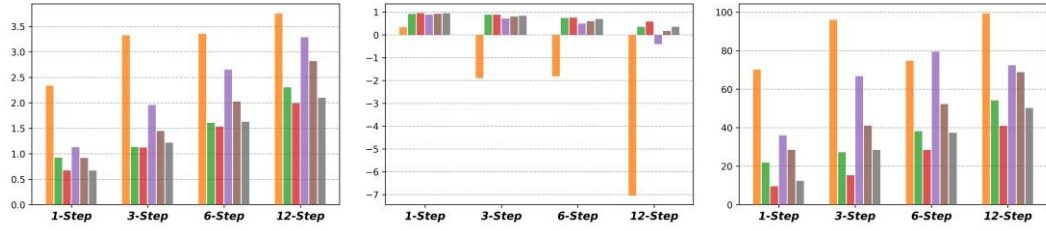


Fig. 7 Average performance results of 30 models for the ETTh1 dataset. RMSE (root mean square error), R^2 (R-squared), and DTW: dynamic time warping

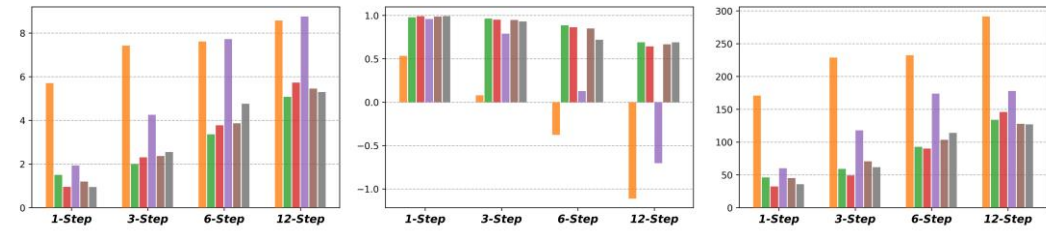


Fig. 8 Average performance results of 30 models for the ETTh2 dataset. RMSE (root mean square error), R^2 (R-squared), and DTW: dynamic time warping

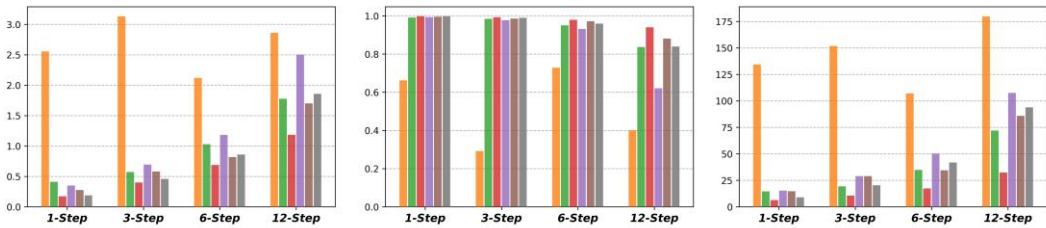


Fig. 9 Average performance results of 30 models for the Weather dataset. RMSE (root mean square error), R^2 (R-squared), and DTW: dynamic time warping

5. Comparative Results on Explainability of Multivariable Time-series Forecasting

This section discusses comparative experiments conducted to output the explainability from the feature and sequence perspectives on the multivariate time series prediction results, which is one of the major advantages of DLFomer. The experimental results are also presented.

5.1. Explainability from a Sequence Perspective

The DLFomer model can explain the significance of each feature in every sequence step of the output sequence, as stated in Eq. (21) in Section 3.4. In Algorithm 3, the x-axis of the attention values reflects the sequence of the individual features in a certain order, and dividing it into sequences represents the influence of each sequence.

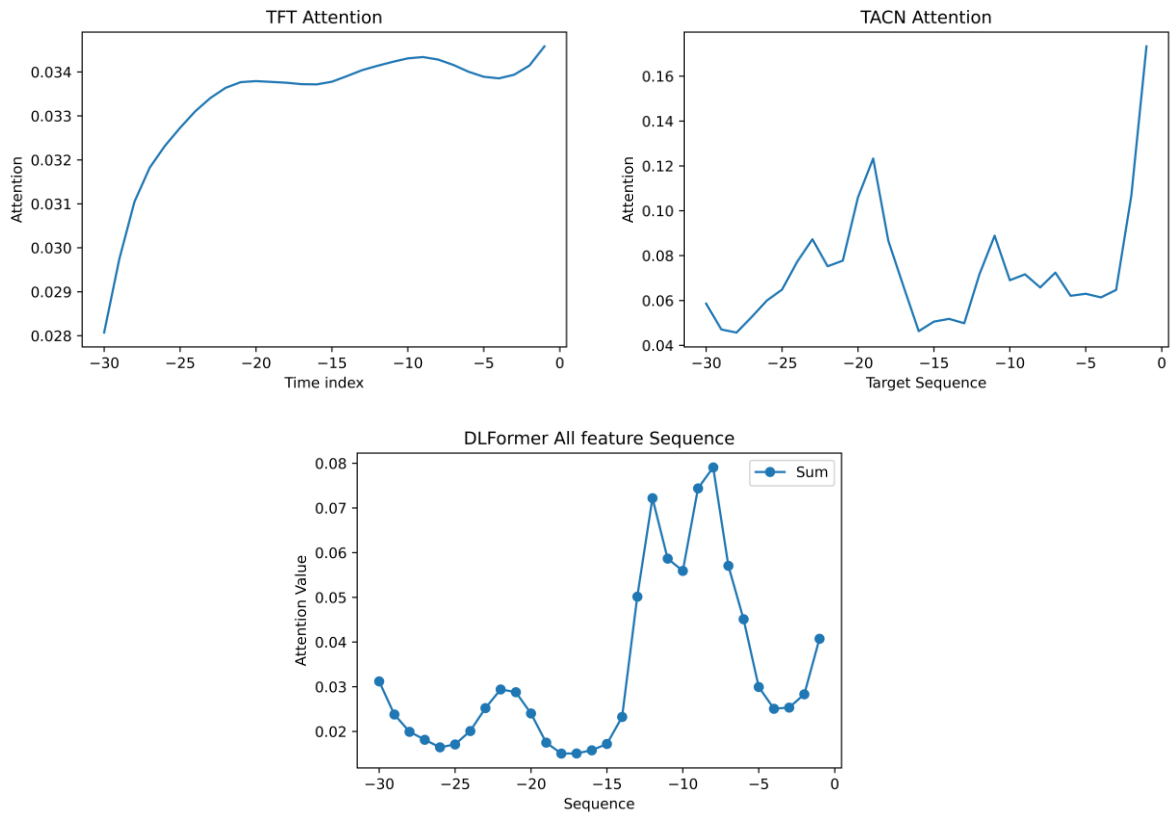


Fig. 10. Interpretation results in terms of sequence perspective in the Air Quality dataset

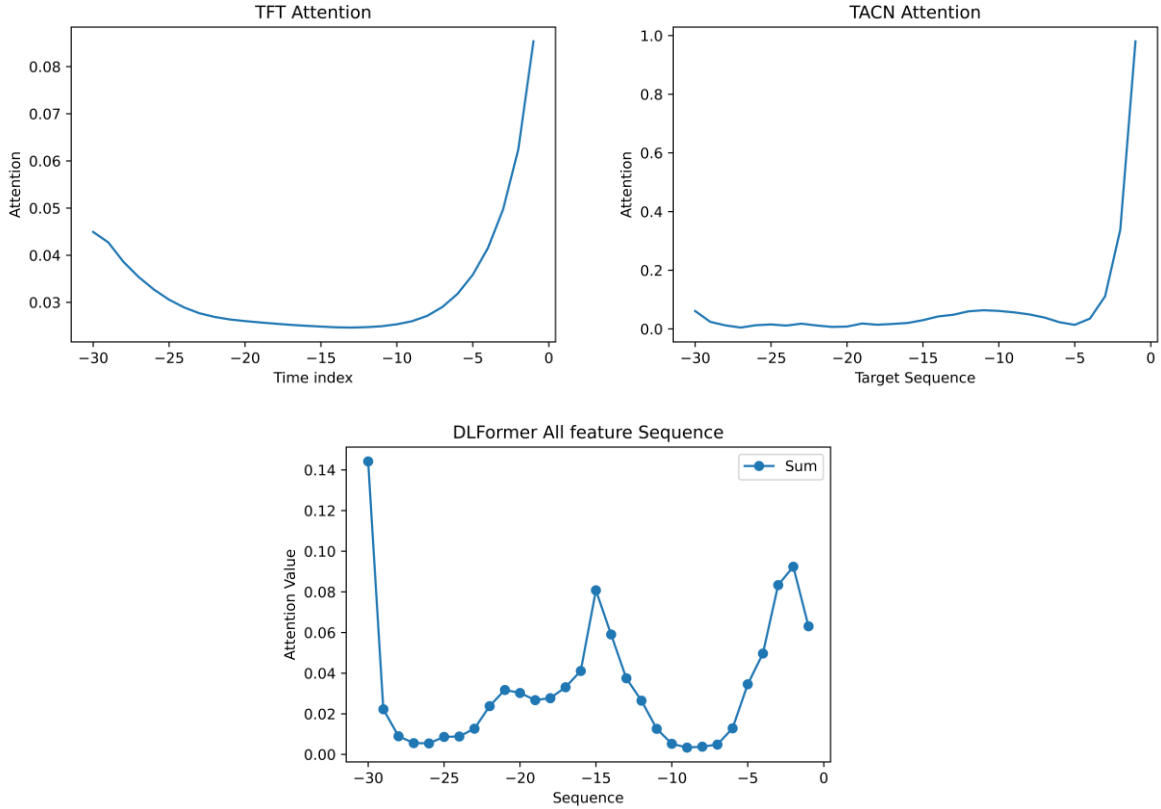


Fig. 11. Interpretation results in terms of sequence perspective in the Weather dataset

Figs. 10 and 11 summarize the individual sequence attention for all features using the Air Quality and Weather datasets, respectively, for comparison with the TFT and TACN, which shows the overall influence of the features in the sequence. The lag and window size parameters were fixed at 30 to ensure equal conditions. The DLFormer, TFT, and TACN models are displayed in order from left to right. In the Air Quality dataset, carbon monoxide (CO) was chosen as the target feature, while in the Weather dataset, temperature ($^{\circ}\text{C}$) was selected. TFT and TACN models show a relatively high influence of the values immediately before the prediction horizon due to their collective representation of the common sequence influence of individual features. This observation is similar to the results obtained by aggregating the attention of all features in the DLFormer. This indicates that DLFormer yields meaningful results when considering the individual sequence of each feature and the common sequence. Furthermore, TFT and TACN exhibit the outcome characteristics of autoregressive models, whereas DLFormer demonstrates a better capture of patterns at crucial time points in previous specific sequences that influence predictions.

Figs. 12 and 13 illustrate the influence of the input sequences of the individual features on DLFormer using Air Quality and Weather datasets, respectively, consistent with previous research. Both exhibit the typical characteristics of autoregressive models, where sequences near the prediction horizon significantly influence the forecasting sequence of the target feature. Moreover, the impact of distant time steps on relatively less significant features is greater than that on the prediction horizon, as proven by the characteristics of attention. In contrast to conventional approaches, DLFormer utilizes distributed lag variables and interpretable multihead attention to precisely represent the impact of each time step of individual features on a target feature. This enables an in-depth understanding of time intervals in forecasting and provides an essential indicator for assessing the potential misapplications of prediction models.

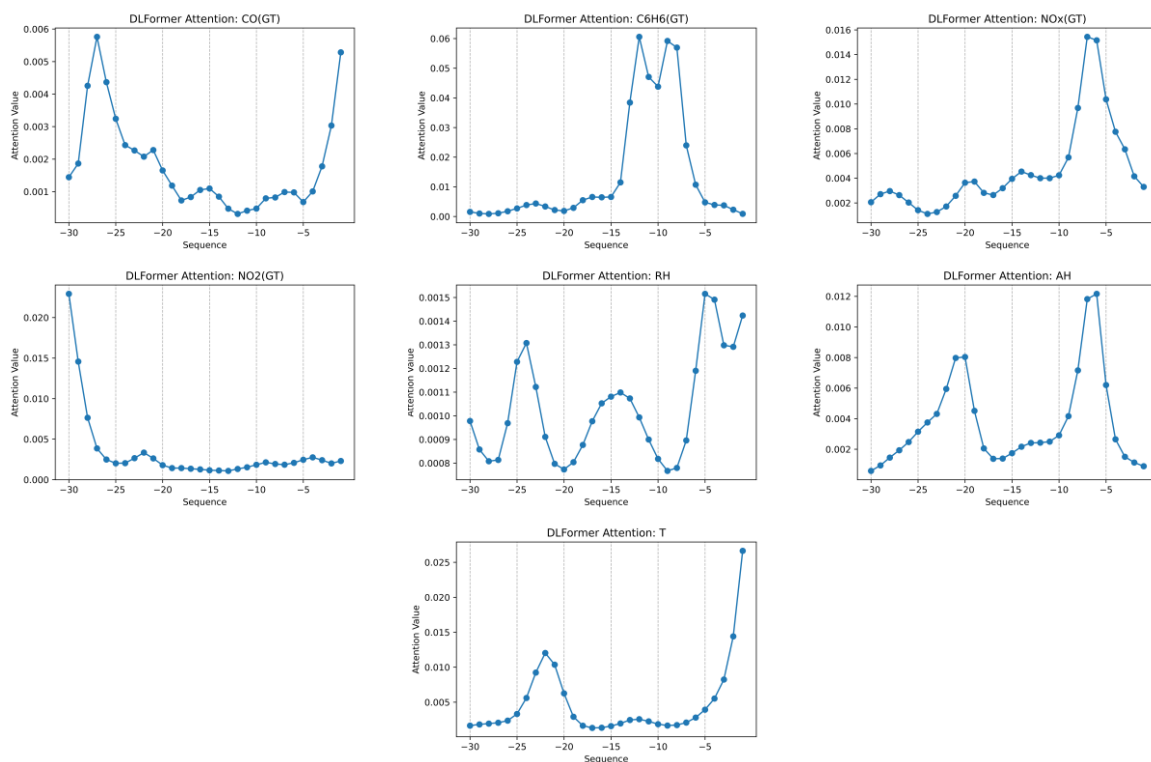


Fig. 12. Interpretation results of DLFormer for individual features from a sequence perspective in the Air Quality Dataset

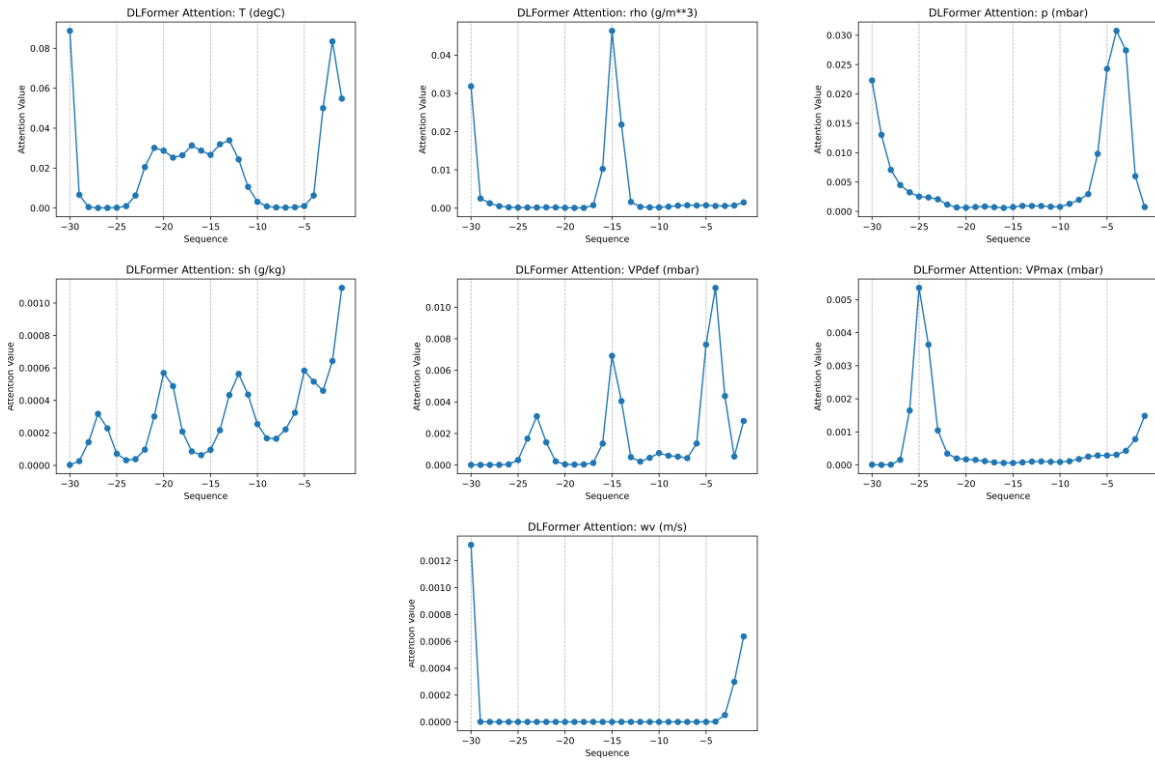


Fig. 13. Interpretation results of DLFormer for individual features from a sequence perspective in the Weather Dataset

5.2. Explainability from a Feature Perspective

Figs. 14 and 15 illustrate the outcomes of the experiments conducted on the Air Quality and Weather datasets, respectively, and demonstrate the significance of the individual features in DLFormer using bar plots. Furthermore, the encoder feature influence results obtained by TFT's Variable variable selection networks are provided for comparison. Fig. 14 illustrates a dataset containing sensor values related to roadways in Italian cities in the Air Quality dataset. As roadway traffic increases, the CO level also increases (Angatha & Mehar, 2020). Both models frequently describe this phenomenon as the increase in benzene (C₆H₆) concentration in tandem with gasoline usage, exerting a substantial mutual influence. In addition, our DLFormer demonstrated high significance values for nitrogen oxides (NO_x), which aligns with the data indicating a significant impact of NO_x on CO oxidation (Glarborg, Kubel, Kristensen, Hansen, & Dam-Johansen, 1995). Fig. 15 shows the temperature and weather data obtained from Germany for the Weather dataset. We again compared the feature influence between DLFormer and TFT, as depicted in Fig. 14. Typically, the past values of the target feature, T (°C), had the most impact, whereas other features provided similar outcomes in both methods. This indicates that the features are more influenced by their values or prior patterns than external influences.

Fig. 16 and 17 show the sequence influence of individual features from the top 20 most influential outputs. The left and right figures show the results using the Air Quality and Weather datasets, respectively. It is feasible to anticipate that the impact of a feature will be more significant than that of a time point. Moreover, the differences in the significance of the 6- and 12-lag in Air Quality and the 30- and 12-lag in T (°C) indicate the importance of considering the individual sequence of the features. Furthermore, as observed in previous studies (Desportes, Andry, Fijalkow, & David, 2019), a 30-lag in the Weather dataset has the highest impact. The results confirm that the attention mechanism is intended to utilize these pattern functions effectively

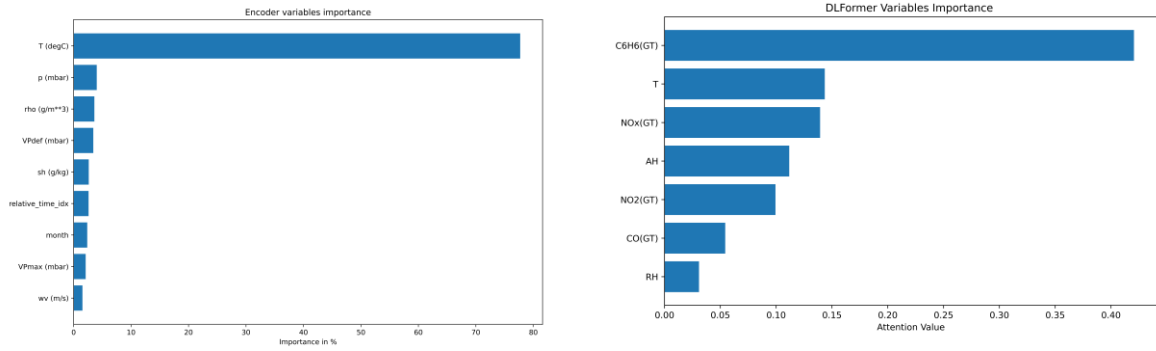


Fig. 14. Interpretation results in terms of feature perspective in the Air Quality dataset

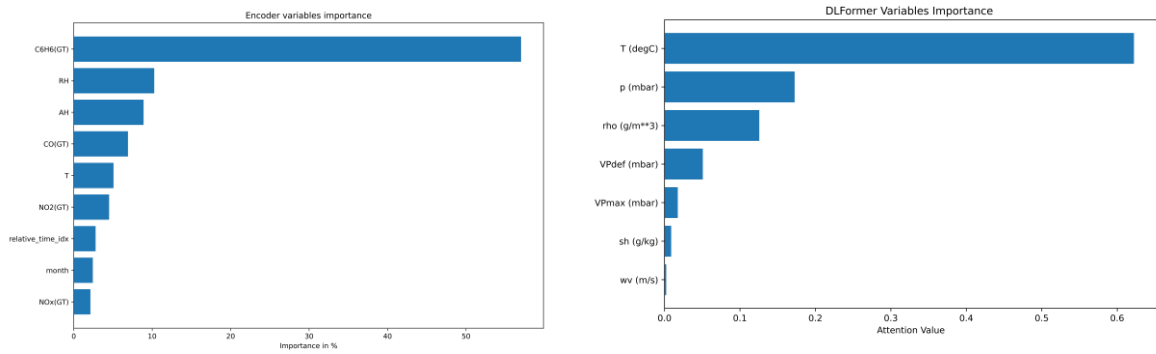


Fig. 15. Interpretation results in terms of feature perspective in the Weather dataset

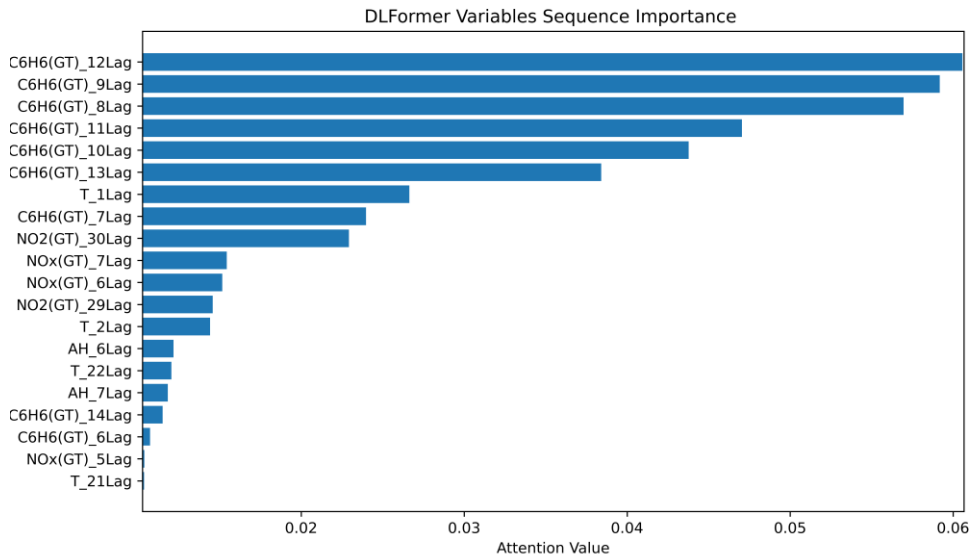


Fig. 16 Interpretation results of DLFormer for individual sequence-feature perspective in the Air Quality dataset

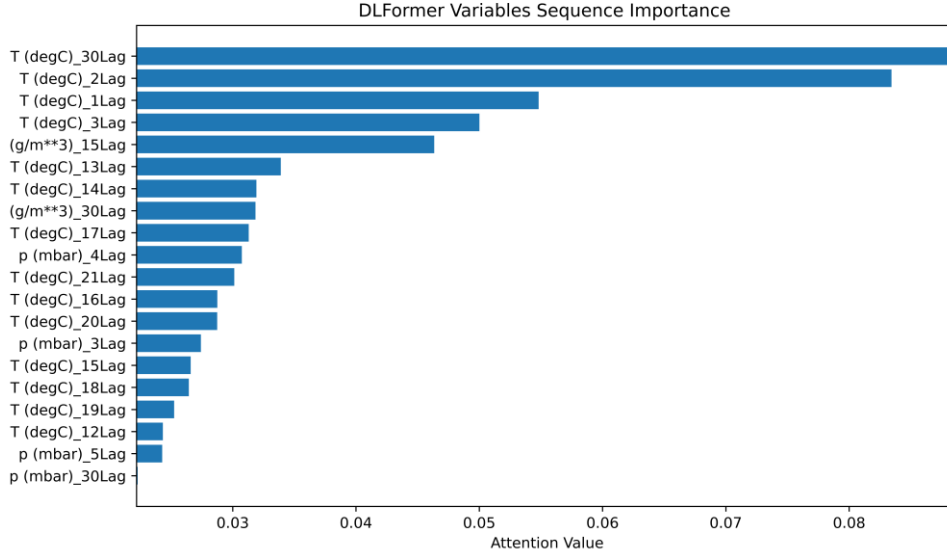


Fig. 16 Interpretation results of DLFormer for individual sequence-feature perspective in the Weather dataset

TFT and TACN can provide distinct intuitive explanations for predictions in addition to earlier explanations. However, these models cannot accurately explain cases where the target feature is influenced by values encompassing multiple sequences of individual features. In contrast, DLFormer provides a high degree of explainability for forecasts in these situations. Thus, the proposed model can identify cases of inaccurate predictions and acquire new insights from the obtained multivariate time series data

6. Conclusions

This study proposes DLFormer, a method that effectively evaluates the influence of each input feature on the predictive attention performance by enhancing the accuracy of multivariate time series forecasting. It primarily consists of the following elements: (1) DLE that considers the influence of all input factors and focuses on learning attention. (2) Interpretable multihead attention to accurately represent the sequential influences of individual features acquired from different heads. We evaluated the DLFormer model using four datasets, including multivariable time series and real-world benchmark data. The results validated a prediction performance comparable to that of the most recent high-performance non-interpretable models. In addition, the attention values of each input feature were displayed separately to illustrate their explainability. In the future, we will develop an architecture that utilizes a learned decoder input to achieve the most effective predictive performance. Additionally, we will investigate methods to reduce temporal complexity while analyzing each input sequence individually.

Acknowledgments

This work was supported by the National Research Foundation of Korea (NRF) grant funded by the Korean government (MSIT) (No.RS-2023-00218913) and by MSIT, Korea, under the Grand Information Technology Research Center support program (IITP-202-2020-0-01791) supervised by the

Institute for Information & Communications Technology Planning & Evaluation and was supported by the BB21plus funded by Busan Metropolitan City and Busan Techno Park

References

- Angatha, R. K., & Mehar, A. (2020). Impact of traffic on carbon monoxide concentrations near urban road mid-blocks. *Journal of The Institution of Engineers (India): Series A*, 101, 713-722.
- Bahdanau, D., Cho, K., & Bengio, Y. (2014). Neural machine translation by jointly learning to align and translate. arXiv preprint arXiv:1409.0473.
- Bellotti, A., Brigo, D., Gambetti, P., & Vrins, F. (2021). Forecasting recovery rates on non-performing loans with machine learning. *International Journal of Forecasting*, 37(1), 428-444.
- Bentzen, J., & Engsted, T. (2001). A revival of the autoregressive distributed lag model in estimating energy demand relationships. *Energy*, 26(1), 45-55.
- Berndt, D. J., & Clifford, J. (1994, July). Using dynamic time warping to find patterns in time series. In *Proceedings of the 3rd international conference on knowledge discovery and data mining* (pp. 359-370).
- Bidarkota, P. V. (1998). The comparative forecast performance of univariate and multivariate models: an application to real interest rate forecasting. *International Journal of Forecasting*, 14(4), 457-468.
- Bildirici, M., & Türkmen, C. (2015). The chaotic relationship between oil return, gold, silver and copper returns in Turkey: Non-linear ARDL and augmented non-linear Granger causality. *Procedia-Social and Behavioral Sciences*, 210, 397-407.
- Catania, L., Grassi, S., & Ravazzolo, F. (2019). Forecasting cryptocurrencies under model and parameter instability. *International Journal of Forecasting*, 35(2), 485-501.
- Chung, J., Gulcehre, C., Cho, K., & Bengio, Y. (2014). Empirical evaluation of gated recurrent neural networks on sequence modeling. arXiv preprint arXiv:1412.3555.
- Clements, M. P., Franses, P. H., & Swanson, N. R. (2004). Forecasting economic and financial time-series with non-linear models. *International journal of forecasting*, 20(2), 169-183.
- Costa, L. D., & Machado, A. M. (2023, August). Prediction of stock price time series using transformers. In *Anais do II Brazilian Workshop on Artificial Intelligence in Finance* (pp. 85-95). SBC.
- Crook, B., Schlüter, M., & Speith, T. (2023, September). Revisiting the performance-explainability trade-off in explainable artificial intelligence (XAI). In *2023 IEEE 31st International Requirements Engineering Conference Workshops (REW)* (pp. 316-324). IEEE.
- Desportes, L., Andry, P., Fijalkow, I., & David, J. (2019). Short-term temperature forecasting on a several hours horizon. In *Artificial Neural Networks and Machine Learning–ICANN 2019: Text and Time Series: 28th International Conference on Artificial Neural Networks, Munich, Germany, September 17–19, 2019, Proceedings, Part IV 28* (pp. 525-536). Springer International Publishing.
- Elalem, Y. K., Maier, S., & Seifert, R. W. (2023). A machine learning-based framework for forecasting sales of new products with short life cycles using deep neural networks. *International Journal of Forecasting*, 39(4), 1874-1894.
- Glarborg, P., Kubel, D., Kristensen, P. G., Hansen, J., & Dam-Johansen, K. (1995). Interactions of CO, NO_x and H₂O under post-flame conditions. *Combustion science and technology*, 110(1), 461-485.
- Gong, D., Medioni, G., & Zhao, X. (2013). Structured time series analysis for human action segmentation and recognition. *IEEE transactions on pattern analysis and machine intelligence*, 36(7), 1414-1427.
- Hochreiter, S., & Schmidhuber, J. (1997). Long short-term memory. *Neural computation*, 9(8), 1735-1780.
- Jin, J., Guo, H., Xu, J., Wang, X., & Wang, F. Y. (2020). An end-to-end recommendation system for urban traffic controls and management under a parallel learning framework. *IEEE Transactions on Intelligent Transportation Systems*, 22(3), 1616-1626.
- Karim, F., Majumdar, S., & Darabi, H. (2020). Adversarial attacks on time series. *IEEE transactions on pattern analysis and machine intelligence*, 43(10), 3309-3320.
- Katsikopoulos, K. V., Şimşek, Ö., Buckmann, M., & Gigerenzer, G. (2022). Reply to commentaries on “transparent modelling of influenza incidence”: Recency heuristics and psychological ai. *International Journal of Forecasting*, 38(2), 630-634.
- Kingma, D. P., & Ba, J. (2014). Adam: A method for stochastic optimization. arXiv preprint arXiv:1412.6980.
- Kim, D., Sim, S., Yoon, B., Liu, L., & Bae, H. (2023, November). Improving Time-Series Classification Accuracy Based on Temporal Feature Representation Learning Using CRU-LSTM Autoencoder. In *2023 IEEE 5th International Conference on Cognitive Machine Intelligence (CogMI)* (pp. 175-183). IEEE.
- Lai, G., Chang, W. C., Yang, Y., & Liu, H. (2018, June). Modeling long-and short-term temporal patterns with

- deep neural networks. In The 41st international ACM SIGIR conference on research & development in information retrieval (pp. 95-104).
- Lee, J., Kim, D., & Sim, S. (2024). Temporal Multi-features Representation Learning-Based Clustering for Time-Series Data. *IEEE Access*.
- Lee, J., Shin, J. H., & Kim, J. S. (2017, September). Interactive visualization and manipulation of attention-based neural machine translation. In *Proceedings of the 2017 Conference on Empirical Methods in Natural Language Processing: System Demonstrations* (pp. 121-126).
- Li, X., Shang, W., & Wang, S. (2019). Text-based crude oil price forecasting: A deep learning approach. *International Journal of Forecasting*, 35(4), 1548-1560.
- Lim, B., & Zohren, S. (2021). Time-series forecasting with deep learning: a survey. *Philosophical Transactions of the Royal Society A*, 379(2194), 20200209.
- Lim, B., Arik, S. Ö., Loeff, N., & Pfister, T. (2021). Temporal fusion transformers for interpretable multi-horizon time series forecasting. *International Journal of Forecasting*, 37(4), 1748-1764.
- López Santos, M., García-Santiago, X., Echevarría Camarero, F., Blázquez Gil, G., & Carrasco Ortega, P. (2022). Application of temporal fusion transformer for day-ahead PV power forecasting. *Energies*, 15(14), 5232.
- Makridakis, S., Hyndman, R. J., & Petropoulos, F. (2020). Forecasting in social settings: The state of the art. *International Journal of Forecasting*, 36(1), 15-28.
- Nair, V., & Hinton, G. E. (2010). Rectified linear units improve restricted boltzmann machines. In *Proceedings of the 27th international conference on machine learning (ICML-10)* (pp. 807-814).
- Ortega, L. C., Otero, L. D., Solomon, M., Otero, C. E., & Fabregas, A. (2023). Deep learning models for visibility forecasting using climatological data. *International Journal of Forecasting*, 39(2), 992-1004.
- Pantiskas, L., Verstoep, K., & Bal, H. (2020, December). Interpretable multivariate time series forecasting with temporal attention convolutional neural networks. In *2020 IEEE Symposium Series on Computational Intelligence (SSCI)* (pp. 1687-1694). IEEE.
- Petropoulos, F., Makridakis, S., & Stylianou, N. (2022). COVID-19: Forecasting confirmed cases and deaths with a simple time series model. *International journal of forecasting*, 38(2), 439-452.
- Qu, B., Huang, Y., She, J., Liao, P., & Lai, X. (2024). Forecasting and early warning of bridge monitoring information based on a multivariate time series ARDL model. *Physics and Chemistry of the Earth, Parts A/B/C*, 133, 103533.
- Rajapaksha, D., Bergmeir, C., & Hyndman, R. J. (2023). LoMEF: A framework to produce local explanations for global model time series forecasts. *International Journal of Forecasting*, 39(3), 1424-1447.
- Raza, N., Shahzad, S. J. H., Tiwari, A. K., & Shahbaz, M. (2016). Asymmetric impact of gold, oil prices and their volatilities on stock prices of emerging markets. *Resources Policy*, 49, 290-301.
- Rumelhart, D. E., Hinton, G. E., & Williams, R. J. (1986). Learning representations by back-propagating errors. *nature*, 323(6088), 533-536.
- Salinas, D., Flunkert, V., Gasthaus, J., & Januschowski, T. (2020). DeepAR: Probabilistic forecasting with autoregressive recurrent networks. *International journal of forecasting*, 36(3), 1181-1191.
- Sim, S., Park, J. H., & Bae, H. (2022). Deep collaborative learning model for port-air pollutants prediction using automatic identification system. *Transportation Research Part D: Transport and Environment*, 111, 103431.
- Sim, S., Kim, D., & Bae, H. (2023). Correlation recurrent units: A novel neural architecture for improving the predictive performance of time-series data. *IEEE Transactions on Pattern Analysis and Machine Intelligence*.
- Sim, S., Kim, D., & Jeong, S. C. (2023, February). Temporal Attention Gate Network With Temporal Decomposition for Improved Prediction Accuracy of Univariate Time-Series Data. In *2023 International Conference on Artificial Intelligence in Information and Communication (ICAIIIC)* (pp. 122-127). IEEE.
- Sprangers, O., Schelter, S., & de Rijke, M. (2023). Parameter-efficient deep probabilistic forecasting. *International Journal of Forecasting*, 39(1), 332-345.
- Vaswani, A., Shazeer, N., Parmar, N., Uszkoreit, J., Jones, L., Gomez, A. N., ... & Polosukhin, I. (2017). Attention is all you need. *Advances in neural information processing systems*, 30.
- Wang, X., Hyndman, R. J., Li, F., & Kang, Y. (2023). Forecast combinations: An over 50-year review. *International Journal of Forecasting*, 39(4), 1518-1547.
- Wilms, I., Rombouts, J., & Croux, C. (2021). Multivariate volatility forecasts for stock market indices. *International Journal of Forecasting*, 37(2), 484-499.
- Wu, B., Wang, L., & Zeng, Y. R. (2022). Interpretable wind speed prediction with multivariate time series and temporal fusion transformers. *Energy*, 252, 123990.

- Wu, H., Xu, J., Wang, J., & Long, M. (2021). Autoformer: Decomposition transformers with auto-correlation for long-term series forecasting. *Advances in neural information processing systems*, 34, 22419-22430.
- Zeng, A., Chen, M., Zhang, L., & Xu, Q. (2023, June). Are transformers effective for time series forecasting?. In *Proceedings of the AAAI conference on artificial intelligence* (Vol. 37, No. 9, pp. 11121-11128).
- Zhou, F., De la Torre, F., & Hodgins, J. K. (2012). Hierarchical aligned cluster analysis for temporal clustering of human motion. *IEEE Transactions on Pattern Analysis and Machine Intelligence*, 35(3), 582-596.
- Zhou, H., Zhang, S., Peng, J., Zhang, S., Li, J., Xiong, H., & Zhang, W. (2021, May). Informer: Beyond efficient transformer for long sequence time-series forecasting. In *Proceedings of the AAAI conference on artificial intelligence* (Vol. 35, No. 12, pp. 11106-11115).